Modeling ionic mobilities by scattering on electronic density isosurfaces: Application to silicon cluster anions

Alexandre A. Shvartsburg[a)]
Department of Chemistry, Northwestern University, 2145 Sheridan Road, Evanston, Illinois 60208

Bei Liu
Ames Laboratory and Department of Physics and Astronomy, Iowa State University, Ames, Iowa 50011

Martin F. Jarrold
Department of Chemistry, Northwestern University, 2145 Sheridan Road, Evanston, Illinois 60208

Kai-Ming Ho
Ames Laboratory and Department of Physics and Astronomy, Iowa State University, Ames, Iowa 50011

(Received 17 August 1999; accepted 27 October 1999)

We have developed a new formalism to evaluate the gas-phase mobility of an ion based on elastic scattering on an electronic density isosurface (SEDI). In this method, the ion is represented by a surface of arbitrary shape defined as a set of points in space where the total electron density assumes a certain value. This value is the only adjustable parameter in the model. Conceptually, this treatment emulates the interaction between a drifting ion and the buffer gas atoms closer than the previously described methods, the exact hard spheres scattering (EHSS) model and trajectory calculations, where the scattering occurs in potentials centered on the nuclei. We have employed EHSS, trajectory calculations, and SEDI to compute the room temperature mobilities for low-energy isomers of Si_n ($n \leqslant 20$) cations and anions optimized by density functional theory (DFT) in the local density approximation and generalized gradient approximation. The results produced by SEDI are in excellent agreement with the measurements for both charge states, while other methods can fit the mobilities for cations only. Using SEDI, we have confirmed the structural differences between Si_n^+ and Si_n^- predicted by DFT calculations, including the major rearrangements for $n=9$, 15, 16, and 18. We have also assigned the multiple isomers observed in recent high-resolution mobility measurements for Si_n^+ with $n=17-19$, some of them to near-spherical cage-like geometries. [S0021-9606(00)01104-1]

I. INTRODUCTION

Mobility measurements have been established over the last decade as a versatile and powerful tool for the structural characterization of gas-phase ions. This approach has been of particular value in elucidating the structure of atomic clusters because spectroscopic methods generally fail to resolve specific features for all but the smallest species.[1] Mobility measurements determine the velocity with which an object drifts through a buffer gas under the influence of an external electric field. Mobilities can be measured for either positively or negatively charged species (but not for the neutrals). Most investigations to date have been carried out on cations. For example, the extensive research on carbon clusters that revealed structural transitions from chains to monocyclic and polycyclic rings to fullerenes,[2–4] and demonstrated the isomerization of carbon rings into fullerenes[5–7] was performed mainly on cations. Carbon clusters doped by various elements (hydrogen,[8] chlorine,[9] silicon,[10] metals[11–14]) have been investigated for cations only. Similarly, the detailed work on aluminum[15,16] and the Group 4 elements (silicon,[17–20] germanium,[21,22] and tin[23]) species was done on cations. More recently, mobility measurements have been used to determine the gas-phase conformations of large bio-organic[24–26] and biological[27–29] molecules. Again, this research has been done mainly on the positively charged ions.

The assignment of features observed in mobility measurements is accomplished by comparison with collision integrals calculated for a number of plausible candidate geometries. Since most of the experimental data available on the mobilities of polyatomic ions are for cations, the computational methods developed to model the mobilities have really only been validated for cations. In order of increasing sophistication (and computational expense), those methods are (i) the projection approximation that equates the collision integral to the orientationally averaged projection,[3,30] (ii) the exact hard spheres scattering[31] (EHSS) model that replaces the collision integral by the orientationally averaged momentum-transfer cross section of a collection of hard spheres, and (iii) trajectory calculations[32,23] where the trajectories of buffer gas atoms are propagated in a realistic molecular potential of the target ion using the methods of molecular dynamics. While the projection approximation produces large errors in many cases,[20,32–35] the EHSS and trajectory calculations have been successful in accurately predicting the mobilities of both homoatomic[19,20,22,32–37] (C_n^+, Si_n^+, Ge_n^+) and heteroatomic[9,14,38–40]

[a)]Present address: Department of Chemistry, York University, 4700 Keele St., Toronto, Ontario, Canada M3J1P3.

($Na_nCl_{n+1}^-$, C_nSi^+, $C_{60}Nb_m^+$) clusters, as well as various bio-organic molecules.[24,25]

Mobility measurements[33,41] have shown that the size ranges of certain structural families are different for C_n^- and C_n^+. Anions also exhibit geometries not observed for cations, such as monocyclic rings with side chains attached (''tadpoles'').[42] For the fullerenes and their dimers, the mobilities of cations and anions with the same geometries are nearly identical.[33–35] Although the cross sections for anions are slightly larger, the difference is nearly constant and so small (<1%) that in the analysis of data it could be treated simply as a systematic empirical correction.[35] This is hardly surprising considering that these clusters have ~50–150 atoms. In free-electron metal clusters, the tail of the electron density extends beyond the ''edge'' of the cluster.[43] The electron density spills out further for anions than for cations. Physically, the buffer gas atoms scatter on the electron cloud of the drifting ion, so the cross sections of anions should be larger than for cations. The mobilities measured[44] for In_n^- are significantly smaller than those for In_n^+. The average difference between the mobilities of In_n^+ and In_n^- has been quantitatively reproduced[44] by the jellium model (in the standard spherical-background SBJM implementation). However, the specific size-to-size differences could not be explained by this model. These are presumably due to the differences in shapes of the cations and anions that are ignored by the SBJM. These differences could possibly be captured by more advanced jellium treatments,[45,46] allowing for the triaxial deformations of electron cloud. However, the collision integrals for resulting irregular bodies could not be computed by any of the methods available from the literature. Recent high-resolution measurements[47] have revealed differences between the mobilities of Si_n cations and anions that are both substantial in absolute terms and highly size dependent. Silicon clusters cannot be adequately described by a jellium model.

Summarizing, the modeling of the gas-phase mobilities of anions has not been explored. Specifically, the assumption that exact hard spheres scattering and trajectory calculations will work for anions as well as for cations has not been verified. The spherical jellium-based approach[44] cannot extract any specific structural information even for the free-electron metal clusters. Hence, there is a need to carefully test the existing methods of mobility calculations on anions and, should they prove inadequate, to devise new approaches. This issue is the subject of present contribution with Si_n anions as the test case. The main reasons for choosing this system are (i) the availability of high-resolution data for cations and anions under identical conditions across a wide range of cluster sizes,[47] (ii) the challenge of modeling the strongly size-dependent differences between mobilities of the two charge states, and (iii) the fact that the geometries of Si clusters are well-defined at room temperature and can be found by an unbiased global search.[19,20] Besides, there exists a great deal of interest in the growth pattern of silicon clusters (see Ref. 20 for a review). We have previously optimized the geometries for Si_n neutrals[19] and cations[20] ($n \leqslant 20$). The resulting prolate structures resemble stacks of Si_n tricapped trigonal prisms (TTP). They have been confirmed by comparison with experimental data on mobilities,[19,20] dissociation energies,[48] and fragmentation pathways[48] for cations, and ionization potentials for the neutrals.[20] The structural elucidation of medium-sized Si_n anions will contribute to our understanding of the unique growth habit of silicon clusters.

II. STRUCTURAL OPTIMIZATION OF CHARGED Si_n CLUSTERS

A. Computational methods

To find the global minima of Si_n neutrals with up to 20 atoms,[19] we used a genetic algorithm and simulated annealing with a new tight-binding potential[49] for energy evaluations. Promising candidates were reoptimized using density functional theory (DFT) with the Vosko–Wilk–Nusair (VWN) local density approximation[19,20] (LDA) functional for exchange and correlation, and with the gradient-corrected functionals[20] Perdew–Wang–Becke 88 (PWB) and Becke88–Lee–Yang–Parr (BLYP). Of these three methods, PWB by far provided the best agreement with the measurements of cohesive energies, ionization potentials, and bond lengths.[20] Simulated annealing had repeatedly failed[19,20,22] to locate the true lowest-energy geometries for $n>12$; hence, for larger sizes the use of a genetic algorithm is critical. Unfortunately, no tight-binding potential analogous to that for the neutrals[49] currently exists for charged clusters. The direct coupling of a genetic algorithm and DFT is computationally prohibitive. So, we have relaxed a number of low-energy neutral isomers of each Si_n ($n \leqslant 20$) for anions without any symmetry constraints. Additionally, we have carried out the simulated annealing for $n<12$ using the Car–Parrinello LDA technique.[50] This combined strategy had been successful[20] in finding the structures for Si_n^+ in the same size range (as well as medium-size Ge_n neutrals and cations[22]) that are in agreement with all available experimental data. In addition, here we have performed simulated annealing for $n>12$ starting from the geometries of low-energy neutrals. This procedure is designed to explore the local basins around stable configurations for any distortions that might lower the energy. All calculations have employed the double numeric basis set with polarization functions as implemented in the all-electron localized-basis DMOL code.[51] Spin-polarization terms were included.

B. Correction of cations

Before proceeding to the results for anions, we have to make a correction to our published findings[20] on the structures of Si_n cations. Regrettably, the symmetry of global minima of Si_n neutrals with $n=5$, 7, and 10 had been inadvertently constrained when annealing these geometries for cations. This prevented Jahn–Teller distortion to lower symmetries (in either LDA or PWB): C_{2v} for Si_5^+ and Si_7^+ vs D_{3h} for Si_5 and D_{5h} for Si_7, and C_s for Si_{10}^+ vs C_{3v} for Si_{10}. Kishi *et al.*[52] and Grein and co-workers[53] have recently found the same distortions for Si_5^+ and Si_7^+ using *ab initio* and density functional methods. So, the global minima for these sizes are actually deeper than those given in Ref. 20 by 0.02–0.04 eV/atom. The refined energies are listed in Table I herein,

TABLE I. Cohesive energies (with respect to the spin-polarized isolated neutral atoms) of the low-energy geometries of $Si_n(n \leqslant 20)$ cations, neutrals, and anions, and mobilities for cations and anions. Global minima (both LDA and PWB) for each charge state are in bold (the geometries lying within 3 meV/atom of each other are treated as degenerate). Measured mobilities are the high-resolution data (Ref. 47) at 295 K. All calculated values are by the SEDI model.

		Cohesive energy, eV						Inverse mobilities, Vs/m^2			
		Cations		Neutrals[a]		Anions		Cations		Anions	
n	Point group	LDA	PWB	LDA	PWB	LDA	PWB	Calc.	Exp.[b,c]	Calc	Exp.
2		**−2.003**	**−2.176**	**1.968**	**1.755**	**3.028**	**2.676**				
3	C_{2v}	**0.203**	**−0.165**	**2.929**	**2.537**	**3.688**	**3.267**			**915**	920
4	D_{2h}	**1.541**	**1.106**	**3.509**	**3.042**	**4.048**	**3.565**	**930**	915	**1040**	1040
5	D_{3h}	2.141	1.642	**3.791**	**3.266**	**4.272**	**3.733**	1020	1005	**1115**	1115
	C_{2v} (I)	2.157	1.665		$\Rightarrow D_{3h}$			1020		⋯	
	C_{2v} (II)	**2.160**	**1.669**					**1020**			
6	D_{4h}	2.692	2.145	**4.001**	**3.439**	4.346	3.778	1105	1105	1210	1215
	C_{2v} (I)[d]	**2.724**	**2.187**	**4.001**	**3.438**		$\Rightarrow D_{4h}$	**1110**		⋯	
	C_{2v} (II)		$\Rightarrow D_{4h}$			**4.362**	**3.789**	⋯		**1210**	
7	D_{5h}	2.988	2.410	**4.147**	**3.555**	**4.418**	**3.828**	1190	1195	**1295**	1295
	C_{2v} (I)	3.000	2.433		$\Rightarrow D_{5h}$			1195		⋯	
	C_{2v} (II)	**3.019**	**2.452**					**1195**			
8	C_{2h}	3.179	**2.596**	**4.090**	**3.491**	4.377	3.752	**1300**	1315	1390	1400
	C_1/C_s[e]	**3.185**	**2.596**	4.016	3.422	4.358	3.736	**1290**		1385	
	C_{3v}	3.033	2.458	4.001	3.407	**4.394**	**3.789**	1325		**1395**	
	C_{2v}	3.094	2.517	4.041	3.445	**4.396**	**3.791**	1310		**1395**	
9	C_{2v} (I)	**3.354**	**2.753**	**4.202**	**3.580**	4.398	3.772	**1375**	1380	1465	1440
	C_1		$\Rightarrow C_{2v}$ (I)			4.440	3.812	⋯		1465	
	C_{2v} (II)	3.332	2.727	4.145	3.527	4.371	3.739	1365		1460	
	C_s (I)[f]	3.284	2.690	4.081	3.466	4.400	3.760	1405		1465	
	D_{3h}	3.224	2.627	4.041	3.415	4.439	3.804	1350		1435	
	C_s (II)		$\Rightarrow C_{2v}$ (II)			**4.449**	**3.819**	⋯		**1440**	
10	C_{3v}	3.527	2.900	**4.329**	**3.682**	**4.553**	**3.897**	1425	1415	**1510**	1520
	C_s	**3.550**	**2.924**		$\Rightarrow C_{3v}$			**1415**		⋯	
	T_d	3.494	2.874	4.260	3.626	4.431	3.781	1455		1550	
	C_{4v}	3.473	2.842	4.244	3.595	4.541	3.874	1410		1505	
11	C_{2v} (I)[g]	3.627	2.985	**4.270**	**3.618**	4.433	3.777	1520	1505	1620	1615
	C_s (I)	**3.667**	**3.029**	**4.269**	**3.620**	4.461	3.803	**1515**		1610	
	C_s (II)	3.622	2.973	4.247	3.593	**4.477**	3.816	1510		**1600**	
	C_{2v} (II)	3.627	2.986	4.219	3.577	**4.480**	**3.821**	1505		**1595**	
12	C_{2v}	3.684	3.034	**4.303**	**3.648**	**4.499**	**3.826**	1615	1600	**1695**	1700
	C_s	**3.694**	**3.040**	4.251	3.593	4.483	3.821	**1595**		1700	
13	C_s	3.746	3.093	**4.303**	**3.634**	**4.538**	**3.860**	1670	1680	**1760**	1775
	C_{3v}	3.734	3.082	4.285	3.624	4.456	3.792	1670		1750	
	C_{2v}	**3.751**	**3.102**	4.278	3.616	4.448	3.782	**1675**		1775	
14	C_s (I)[h]	**3.842**	**3.181**	**4.348**	**3.677**	4.505	3.830	**1745**	1755	1845	1850
	C_s (II)	3.769	3.114	4.289	3.621	**4.534**	**3.860**	1770		**1855**	
15	C_{3v}	**3.891**	**3.225**	**4.378**	**3.701**	4.515	3.837	**1845**	1840	1945	1915
	C_s (III)		$\Rightarrow C_{3v}$			**4.538**	**3.862**	⋯		**1945**	
	D_{3h}	3.878	3.197	**4.377**	3.688	4.489	3.789	1760		1850	
	C_s (I)[i]	3.878	3.203	4.367	3.684	**4.536**	3.848	1795		**1895**	
	C_s (II)[i]	**3.894**	3.219	4.366	3.685	**4.539**	3.851	**1795**		**1895**	
16	C_{2h} (I)	3.909	3.236	**4.339**	3.659	4.482	3.800	1925	1930	2035	2010
	C_{2h} (II)	**3.925**	**3.265**	**4.338**	**3.672**	4.508	3.837	**1950**		2055	
	C_s	3.906	3.240	**4.336**	3.661	**4.544**	**3.865**	1925		**2035**	
	C_{3v}	3.917	3.232	4.334	3.642	4.468	3.772	1840		1935	

TABLE I. (*Continued.*)

		Cohesive energy, eV						Inverse mobilities, Vs/m^2			
		Cations		Neutrals[a]		Anions		Cations		Anions	
n	Point group	LDA	PWB	LDA	PWB	LDA	PWB	Calc.	Exp.[b,c]	Calc	Exp.
17	C_{3v}	**3.970**	**3.298**	**4.383**	**3.703**	4.533	3.850	**2010**	1985(1)	2130	2105
	C_s (I)	3.957	3.287	4.359	3.681	**4.548**	**3.869**	2015	2050(2)	**2120**	
	C_2	**3.971**	3.291	4.364	3.675	4.521	3.825	**1925**	1935(3)	2010	
	C_s (II)	3.955	3.281	4.343	3.664	4.475	3.794	2020		2135	
18	C_{3v}	**4.013**	**3.340**	**4.401**	**3.720**	4.513	3.830	**2170**	2115(1)	2270	2155
	D_{3h}	4.006	3.329	4.389	3.704	**4.573**	**3.881**	2095	2155(2)	**2185**	
19	C_{2v}[j]	**4.058**	**3.369**	**4.412**	**3.715**	**4.561**	**3.860**	**2070**	2200(1) 2165(2)	**2175**	2265
	C_s	4.037	3.357	4.396	3.709	4.545	3.854	2195	2075(3)	2300	
20	C_s	**4.081**	**3.388**	**4.416**	**3.714**	4.554	3.848	**2145**	2245	2245	2330
	C_2	4.061	3.381	4.399	**3.712**	**4.559**	**3.866**	2295		**2395**	

[a]The LDA energies of neutrals in the table differ from those listed in Ref. 19 by a small constant shift due to our use of a different local density functional code.
[b]The experimental mobilities listed here for certain cations deviate slightly from those reported previously (Ref. 20). The present values result from the high-resolution measurements (Ref. 47) and thus are deemed more accurate than those obtained using the injected drift tube technique (Ref. 20).
[c]For sizes where multiple isomers have been resolved (Ref. 47) (cations with $n=17-19$), the ordering of their abundances is given in parentheses (from 1 to 3).
[d]Same as C_{2v} in Ref. 20.
[e]This isomer (capped pentagonal bipyramid) has a C_s symmetry for cation and C_1 for the neutral.
[f]Distorted tricapped octahedron, identical to C_s in Refs. 19 and 20.
[g]Identical to C_{2v} in Refs. 19, 20, and 22.
[h]Same as C_s in Refs. 19 and 20.
[i]C_s (II) is identical to the isomer labeled in Ref. 20 as C_1, and C_s (I) is a minor distortion of that structure.
[j]Same as the near-spherical geometry denoted in Ref. 19 as C_s.

and the revised geometries are depicted in Fig. 1. These very minor relaxations do not noticeably influence the calculated mobilities, so the comparison of theoretical values with the measurements in Table I of Ref. 20 remains unaffected. The corrections do not alter the computed adiabatic ionization potentials,[20] because the lowest-energy isomers for Si_5^+, Si_7^+, and Si_{10}^+ are *separate* local minima from those retaining the higher symmetries of respective neutrals. (This is why the relaxation of the neutral geometries for the cations[20] did not yield the global minima.) However, the calculated dissociation energies of the cations and their fragmentation patterns[48] are affected by the small increase in the cohesive energies of Si_5^+, Si_7^+, and Si_{10}^+. Specifically, the agreement with experiment is improved.[54]

C. Structures of Si_n anions

The results of structural optimization for Si_n in all three charge states using LDA and PWB are summarized in Table I. The lowest-energy geometries of Si_n^+, Si_n, and Si_n^- for all $n\leqslant 20$ are depicted in Fig. 1. A remarkable consistency between the local density and gradient-corrected functionals in the energetic ordering of the isomers for all sizes that we had previously noted[20] for neutrals and cations also extends to anions. However, for all charge states in the $n=15-20$ range, gradient corrections favor the more elongated geometries (those with larger cross sections) by 0.01–0.02 eV/atom. This slight shift has also been observed in other studies.[55] PWB bond lengths are uniformly longer than the LDA ones, by ~1.5% regardless of cluster charge.

Small ($n\leqslant 10$) Si_n anions have been optimized in LDA by Chelikowsky and collaborators[56–58] and using *ab initio* methods by Raghavachari and Rohlfing[59–61] and by Kaya and co-workers.[52,62,63] Over the size range of comparison, our conclusions agree with those results. That is, the global minima are identical to those of the neutrals for $n=3$ (C_{2v} triangle), $n=4$ (D_{2h} rhombus), $n=5$ and 7 (D_{3h} trigonal and D_{5h} pentagonal bipyramids, respectively), and $n=10$ (C_{3v} tetracapped trigonal prism). The ground state for Si_6^- is the C_{2v} (II) bicapped tetrahedron. All the geometries above are in agreement[56,57] with the measured photoelectron spectra to the extent one can judge on the basis of electronic band profiles.[64] The structures for $n=3-5$ and 7 have also been confirmed more specifically by vibrationally resolved spectra.[65–68] The accepted *ab initio* geometry for Si_8^- is the C_{3v} tetracapped tetrahedron[59] that is lower in energy than the C_{2h} distorted bicapped octahedron (ground state of the neutral) by 0.35 eV (0.30 eV in PWB). In DFT calculations (either LDA or PWB), a tiny distortion of the C_{3v} morphology to C_{2v} point group slightly lowers the energy. The global minimum for Si_9 anion is the C_s (II) distorted TTP[59] that lies below the D_{3h} TTP by 0.10–0.15 eV in DFT (0.13 eV in *ab initio*). This morphology is totally different from the C_{2v} (I) capped Bernal's structure of the neutral.[19,20,69,70] For larger ($10<n\leqslant 18$) Si_n^-, we find the neutral ground states[19,20] to be preserved for $n=12$ and 13 (respectively,

C_{2v} and C_s). The lowest-energy geometries for Si_{15}^- (in PWB) and Si_{17}^- are only slightly distorted to the C_s symmetry from the C_{3v} global minima for the neutrals, although the latter exist as separate local minima. In LDA, this Si_{15}^- C_s (III) morphology is essentially isoenergetic with the C_s (I)/C_s (II) double-well minimum that is lowest in energy for the Ge_{15} neutral and cation.[22] The lowest-energy geometry for Si_{11} anion, C_{2v} (II), differs from that of either neutral [C_{2v} (I)[71] or C_s (I)] or cation [C_s (I)]. The C_s (II) global minimum for Si_{14} anion is also quite different from the C_s (I) geometry of neutral and cation. For $n=16$ and 18, the second-lowest energy isomers for the neutral and cation (C_s and D_{3h}) become the global minima for anion. The geometries of the anions are the same as for the cations[20] (except for the Jahn–Teller distortions) for $n=3-5$, 7, 10, and 17. For $n=6$, 8, and 11, the structures for Si_n^+, Si_n, and Si_n^- are all different. Except for $n=15$ mentioned above, LDA and PWB yield the same Si_n^- ($n\leqslant 18$) global minima.

Previous calculations[19,20] for Si_n and Si_n^+ have pinpointed a structural transition from prolate TTP stacks to near-spherical cage-like clusters starting at $n=19$. On the basis of data for $n=17$, 19, and 20, the ''prolate'' family becomes more favored on going from cations to neutrals to anions. In fact, the ''prolate'' geometry is clearly the global minimum for Si_{20}^-. To understand this trend, one has to recall that the conversion to ''spherical'' structures is driven by the energy gain obtained by tying up the dangling bonds on Si_9 TTP subunits. The addition of electrons satisfies some of these bonds, thus benefitting the stacked TTP geometries. The rearrangement from Si_9^+ C_{2v} (I) to Si_9^- C_s (II) is apparently driven by the same mechanism.

III. MOBILITIES OF Si_n IONS

A. Mobilities determined by trajectory calculations and EHSS model

Trajectory calculations[32,33] have been quite successful in computing the mobilities for Si_n cations.[20] The effective potential employed in these calculations is constructed as a sum of pairwise Lennard-Jones interactions of He with each clus-

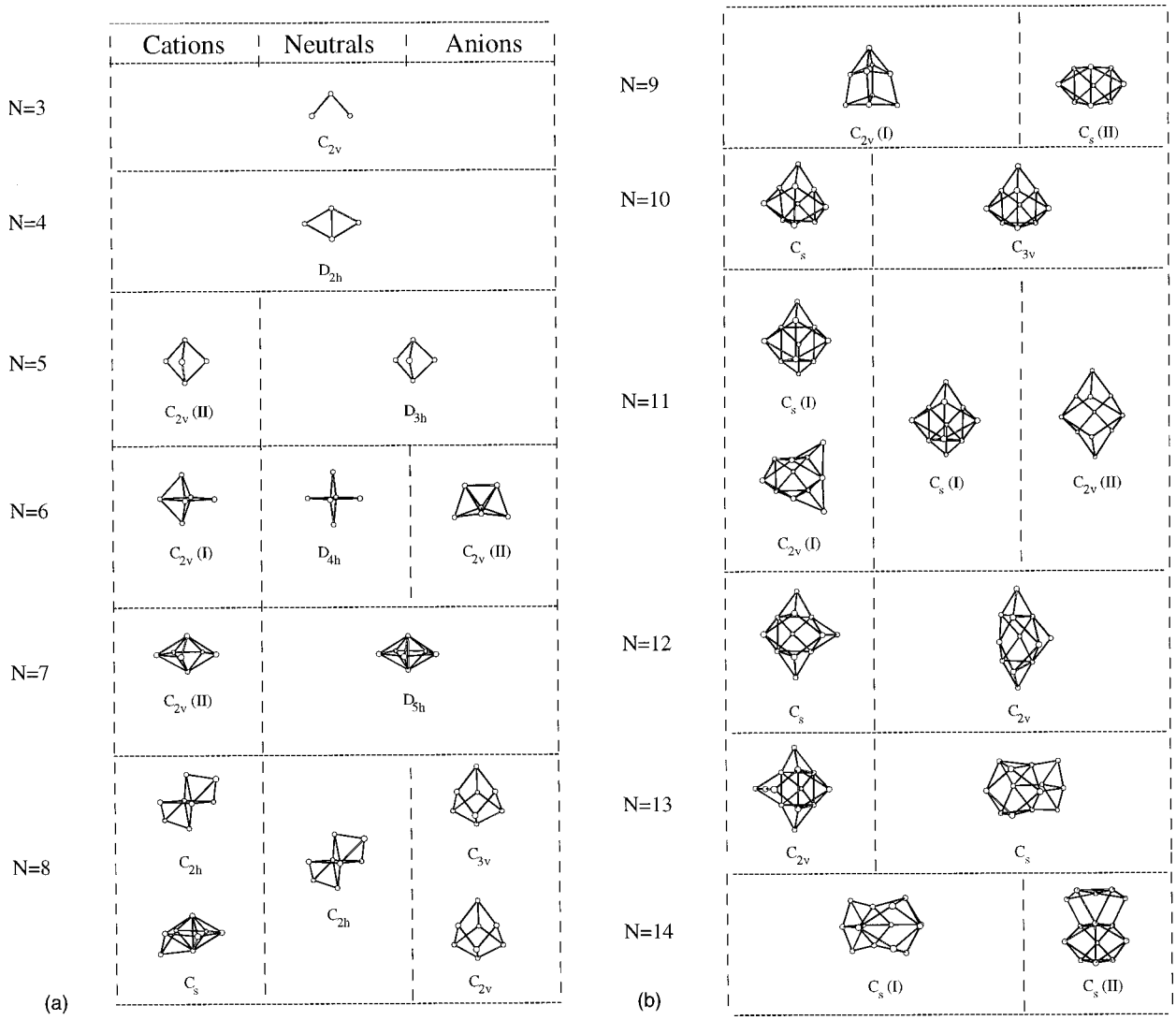

FIG. 1. PWB global minima for the Si_n cations, neutrals, and anions ($n=3-18$). For Si_{15}^-, the C_s (I)/C_s (II) minimum (lowest energy in LDA) that is in agreement with the mobility measurement is added. For $n=19$ and 20, the lowest-energy prolate ''stacked TTP'' structures that we found are shown. Multiple entries mean that the geometries are degenerate within the computational accuracy (~3 meV/atom).

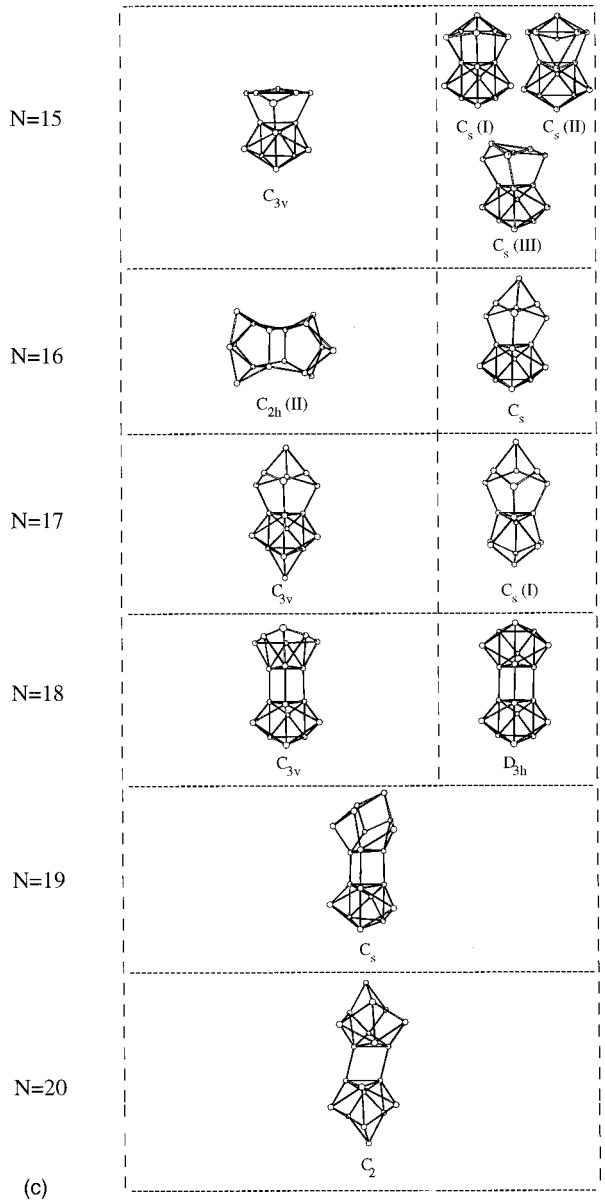

FIG. 1. (*Continued.*)

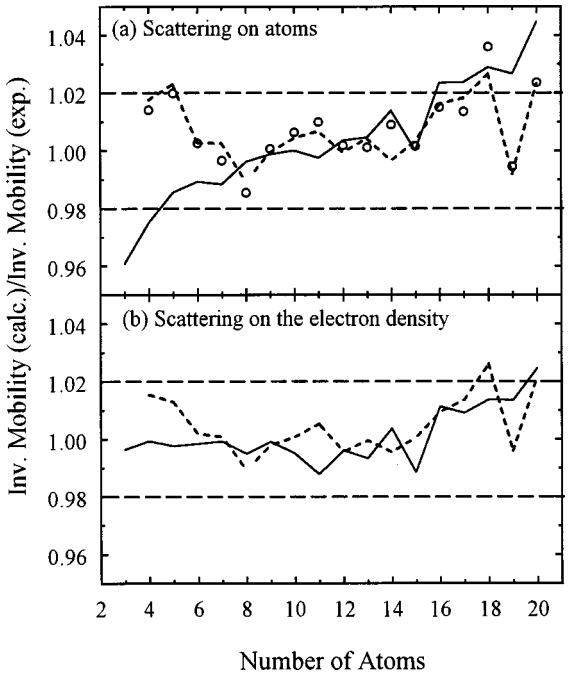

FIG. 2. Inverse mobilities calculated for the lowest-energy [PWB except C_s (I)/C_s (II) geometry for Si_{15}^-] Si_n cations (dotted line) and anions (solid line) in Fig. 1 relative to the high-resolution measurements (for the dominant isomers) (Ref. 47). The C_{2h} isomer is chosen for Si_8^+. Lines in graph (a) result from the exact hard spheres scattering (EHSS) model (Ref. 31) and those in (b) from the scattering on electron density isosurfaces (SEDI). Circles in (a) are by the trajectory calculations (Ref. 20) but the values for some sizes deviate slightly from those given in Ref. 20 because of the more accurate experimental data now available (Ref. 47). Dashed lines delimit the customary 2% error margin (Refs. 3, 11).

ter atom plus a charge-induced dipole term. Recently, we determined the collision integrals of Si_n^+ with He at room temperature using the simpler exact hard spheres scattering model.[31] This treatment is equivalent to a pair-wise hard-sphere potential with no attractive long-range interaction. The Si–He collision radius for EHSS was fit[72] to produce the mobility of Si_7^+ measured[47] at 295 K yielding the value of $R_{\text{cation}}=2.92$ Å. Surprisingly, the mobilities calculated by two methods for all Si_n^+ isomers in the $n=4-26$ size range that we considered agree to within 1%, see for example Fig. 2(a).[73] So, the mobilities for lowest-energy Si_n^+ ($n=4-17$) isomers resulting from both trajectory calculations[20] and the EHSS are within the customary 2% error margin[3,11] of the room temperature measurements.[74] This had not been expected because EHSS is grossly inadequate in modeling the mobilities for carbon clusters (producing errors of over 20% for linear chains), and the trajectory calculations do much better.[33] Of course, the structures of Si_n are less diverse than those of C_n, which renders the interaction potential encountered by a buffer gas atom during a collision to be more consistent across all geometries considered. Also, the range of sizes that we have studied for Si_n is narrower. These two circumstances, however, cannot explain the difference in the performance of EHSS for carbon and silicon species. The key factor apparently is the typical interatomic distance in a cluster. The average Si–Si bond length in Si_n is $L\sim 2.5$ Å, while the C–C bond length in C_n is $L\sim 1.3-1.4$ Å. Hence, a buffer gas atom can interact with more atoms simultaneously in a carbon cluster than in a silicon cluster. For this reason, the cumulative long-range C_n–He potential deepens substantially with increasing n and is strongly dependent on the cluster shape. Conversely, He can interact strongly with only a few neighboring Si atoms at a time; thus, the Si_n–He potential is only weakly affected by the size and shape of cluster as a whole. Thus, the Si–He collision radius, that incorporates the local environment, is transferable across all Si cluster geometries.

If the above hypothesis is correct, the EHSS model should be accurate for all ions with interatomic distances at least as large as those in Si_n. Indeed, good agreement between the results of trajectory calculations and EHSS (at room temperature) is obtained for Ge ($L\sim 2.7$ Å) and Sn ($L\sim 3$ Å) cluster cations.[75] Similarly, the EHSS model correctly predicts the mobilities for Na_nCl_{n+1} ($L\sim 2.8$ Å).[38–40] So, we have attempted to use this model in the analysis of

the mobilities for Si_n^-. The cross sections of Si_n^- systematically exceed those of Si_n^+,[47] thus a larger Si–He collision radius is needed to match experiment. Fitting the room temperature mobility measured[47] for Si_{10}^- (a size in the middle of $n=3-18$ range) yields $R_{\text{anion}}=3.09$ Å. We have reevaluated the collision integrals for all Si_n^- geometries presented in Table I assuming this value for R_{anion}. The mobilities for the global minima of the anions are compared with experiment[47] in Fig. 2(a). It is clear from the figure that the calculated inverse mobility (a quantity proportional to the cross section) increases faster as a function of cluster size than the measured value. This difference persists if one fits R_{anion} for some size other than $n=10$. Hence, the mobilities measured for Si_n anions cannot be accurately modeled with *any choice* of Si–He collision radius.

B. Evaluating mobilities by scattering on electronic density isosurfaces

The exact hard spheres scattering model and the trajectory calculations have one critical feature in common: both assume the scattering to occur in a potential tied to the position of cluster *nuclei*. However, physically the buffer gas atoms scatter on an ion by interaction between *electrons*. As a rigorous quantum calculation involving the electronic wave functions is entirely out of question for the objects of size considered here, our approach involves the classical scattering of buffer gas atoms on the electronic cloud described by a vertical wall of infinite height. The wall is positioned at a certain value of the total electron density, E_{cut}, obtained from calculations. This quantity is the only free parameter in the model. It is adjusted to fit the measurement for one ion with a known geometry and then transferred to other species. This is conceptually analogous to the EHSS model,[31] with E_{cut} substituted for the collision radius R. The electron density isosurfaces generally have irregular shapes. So, we define them numerically on a three-dimensional grid of variable size. The mesh is made finer until the calculated collision integral converges. This is typically attained when the mesh size goes below 0.1 Å. Thus, many thousands of points are needed to appropriately delimit the isosurface even for a small ion. This makes the computational expense of this scattering on the electron density isosurfaces (SEDI) model comparable to that of trajectory calculations.[32–38] While SEDI could be used with many methods of structural optimization, DFT is particularly suitable as it operates directly with the electron density. The SEDI treatment obviously ignores the long-range attractive potential between the ions and buffer gas. So, SEDI should fail like EHSS in cases where these interactions significantly affect the mobilities, carbon clusters being an example.[32,33] Since we have shown these effects to have a negligible impact on the mobilities for Si_n cations, SEDI should be appropriate for this system. And indeed, the SEDI mobilities are within 1% of both EHSS and trajectory calculation values for all Si_n^+ geometries ($n=4-20$) that we considered [Fig. 2(b)].[76] In fact, the SEDI mobilities for lowest-energy Si_n^+ isomers agree with the room-temperature measurements[47] slightly better than those obtained by either of the other two methods. The key point, however, is that the mobilities for global minima of Si_n anions evaluated by SEDI are, unlike those calculated by EHSS, in excellent agreement with experiment,[47] remaining within 2% of the measurements for all sizes considered [Fig. 2(b)].

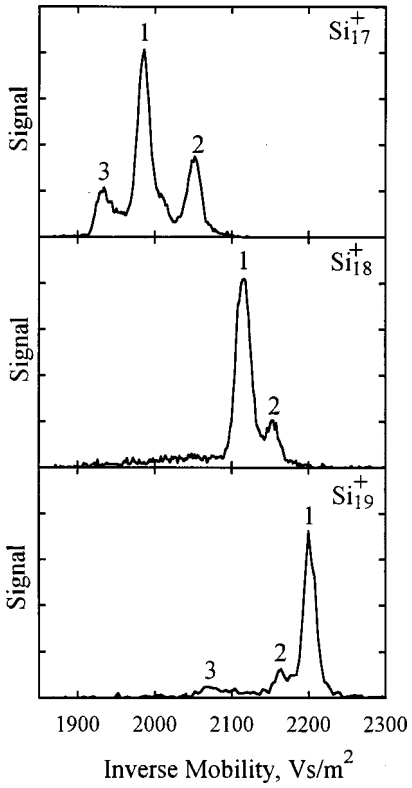

FIG. 3. High-resolution drift time distributions (Ref. 47) for Si_n^+ ($n=17-19$) with multiple isomers resolved.

C. Structural assignments for Si_n cations and characterization of "spherical" geometries

The structural assignments[20] for Si_n cations made on the basis of injected-drift tube measurements and trajectory calculations are fully supported by new, more accurate high-resolution data[47] and the SEDI analysis (see Table I). However, the improved resolution enables us to add to the earlier findings. The mobilities calculated for C_{2h} distorted bicapped octahedron and C_s capped pentagonal bipyramid competing for the ground state of Si_8^+ are so close that they could not be distinguished previously.[20] Our present data virtually exclude the C_s geometry.

For $n=17-19$, two or three geometries are now resolved[47] instead of just one.[20] This is apparent in the drift time distributions for these sizes plotted in Fig. 3. For Si_{17}^+, the lowest and the third-lowest energy isomers [C_{3v} and C_s (I), Fig. 1] fit the major peak in the middle and the second-lowest energy isomer (C_2, Fig. 4) fits the smallest peak at the shortest drift time. The assignment for the second-highest peak at the longest drift time is less solid. It may correspond to the fourth-lowest C_s (II) isomer shown in Fig. 4 (the three other Si_{17}^+ geometries that we found within 1 eV above the ground state are much further away towards shorter drift times). We have pointed out[20] that the mobility for lowest-

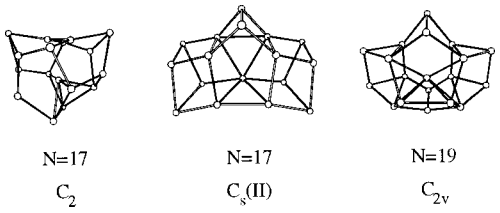

FIG. 4. Low-energy isomers for Si_n^+ ($n=17-19$) possibly observed in the high-resolution mobility measurements (Ref. 47).

energy Si_{18}^+ geometry (C_{3v}, Fig. 1) does not match the measurement, but the mobility for the second-lowest energy isomer (D_{3h}, Fig. 1) does. Two peaks are now resolved[47] for this size: the one at the shorter drift time is assigned as D_{3h} and the other one as C_{3v}. The D_{3h} isomer is the global minimum for Si_{18} anion. For $n=19$, DFT indicates the coexistence of cage-like C_{2v} structure (Fig. 4) with the ''stacked TTP'' isomer (Fig. 1). The ordering of the free energies depends on the entropic contribution.[20] Our previous measurements[20] found only a single peak that was assigned to the prolate geometry. In the recent high-resolution measurements two minor features were resolved at shorter drift times, the left-most of which has exactly the mobility expected for the ''spherical'' Si_{19}^+. The present assignment of minor features in the drift time distributions for Si_{17}^+ and Si_{19}^+ to the cage-like isomers is the first specific structural elucidation of species belonging to the ''spherical'' family that extends to the largest Si clusters examined by mobility measurements[17,18,47] ($n\sim 90$).

D. Structural rearrangements between Si_n cations and anions

In Fig. 5, we plot the absolute difference between the inverse mobilities of Si_n^- and Si_n^+ with $n\leqslant 20$. The difference measured[47] for most sizes is in a narrow band around 100 Vs/m^2. This difference is caused by a systematic expansion of electronic cloud on going from cations to anions due to the two extra electrons. However, there are size-dependent features on top of this overall shift. The SEDI calculation for the lowest-energy geometries of both Si_n^+ and Si_n^- [assuming C_s (I)/C_s (II) isomer for Si_{15}^-] clearly reproduces all major minima in the graph for $n<19$: $n=9$, 15, 16, and 18 (Fig. 5). These deviations from the ≈ 100 Vs/m^2 level are caused by the anion having a more compact geometry than the cation.

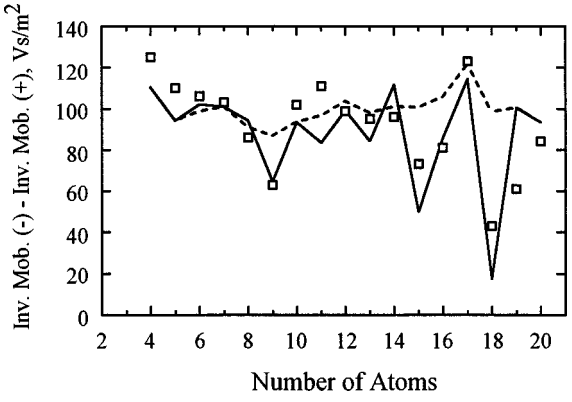

FIG. 5. Gap between the inverse mobilities for Si_n^+ and Si_n^-. Squares are from the high-resolution measurements (for the dominant isomers) (Ref. 47) and the lines are by SEDI calculations. The solid line corresponds to the assumption that the clusters in both charge states adopt their lowest-energy geometries [PWB, except that we have chosen the C_s (I)/C_s (II) isomer for Si_{15}^-; Si_8^+ is assumed to have the C_{2h} structure]. The dashed line would be produced if the morphologies for Si_n anions were identical to those of global minima for cations save for a local relaxation.

To ensure that the features in Fig. 5 are indeed induced by the structural transitions between Si_n^+ and Si_n^- (rather than, for instance, being a manifestation of some effect governed by the number of electrons), we have relaxed the Si_n^+ global minima for anions and evaluated their collision integrals using SEDI. The resulting inverse mobilities differ from those of cations by a constant shift of approximately 100 Vs/m^2, with none of the experimental features reproduced (see Fig. 5). This verifies the C_s (II) TTP for Si_9^-, C_s (I)/C_s (II) isomer for Si_{15}^-, and C_s and D_{3h} geometries for Si_{16}^- and Si_{18}^-, respectively. The Si_9 TTP cluster anions have recently been observed in bulk as a part of the crystal structure for $Rb_{12}Si_{17}$.[77] The cross sections are not appreciably affected by the structural rearrangements between Si_n^+ and Si_n^- for $n=8$ and 11–14, so these unfortunately could not be revealed even by the high-resolution mobility measurements. The mobility measurements for anions exclude the distorted tricapped octahedron Si_9 C_s (I) and tetracapped octahedron Si_{10} T_d extensively discussed in the literature.[71,78–81] In fact, all previously proposed non-TTP geometries for the medium-sized Si clusters (icosahedra,[82–85] ''stacked puckered sixfold rings,''[86–88] ''alternating stacked triangles,''[89,90] ''TBN'' species retaining the ''adamantane'' tetrahedral bonding network of bulk Si,[91] etc.) are ruled out by the measurements for anions as they have been for cations.[20]

As mentioned in Sec. II C, the DFT results suggest that the negative charge favors the ''prolate'' Si_n geometries over the ''spherical'' ones. This should delay the rearrangement to more compact structures in the anions compared to cations. Indeed, the mobility measurements for Si_n^- ($n=17-19$) show no ''spherical'' isomers observed for Si_n^+ with the same n, and the transition region is shifted to larger sizes.

IV. CONCLUSIONS

We have performed a systematic ground-state geometry search for Si cluster anions with up to 20 atoms using density functional theory. The results of local density and gradient-corrected formulations are nearly identical. Overall, the structures adhere to the ''stacked tricapped trigonal prism'' growth pattern established previously for the Si_n neutrals and cations, but the geometries for most sizes differ in detail. The ionic mobilities for the lowest-energy Si_n^- isomers calculated using previously known methods systematically disagree with the measurements.

To remedy this situation, we have developed a new method to calculate mobilities. In this method, the ion is represented by a hard body of arbitrary shape delimited by an irregular three-dimensional surface. This surface is defined numerically on a grid mesh using a cutoff value for the total electron density. The collision integral is computed by

elastic scattering of buffer gas atoms on this surface. The mesh size is decreased until the result converges.

Application of the SEDI model to *both* Si_n cations and anions has yielded mobilities in excellent agreement with experiment. This has enabled us to characterize the structure of medium-size Si_n anions and to confirm all the structural differences between cations and anions in this size range that are predicted by the first-principles optimization. This proves that our optimization methods yield the true Si_n geometries regardless of charge, which amounts to a strong circumstantial evidence that the structures we found for neutrals[19,20] are also right. One may expect the new SEDI method laid out in this contribution to critically enhance the power of mobility measurements as a tool for structural elucidation of negatively charged ions.

ACKNOWLEDGMENTS

We thank Professor K. J. Chang, Professor F. Grein, Dr. J. W. Jeong, Professor K. Kaya, Dr. R. Kishi, Professor C. R. Zacharias, and Dr. M. Woeller for providing us with their optimized geometries of Si clusters, and Dr. W. T. Chan, Dr. Ph. Dugourd, Dr. J. Grossman, Dr. R. R. Hudgins, Professor K. A. Jackson, Professor R. Fournier, and Professor M. A. Ratner for useful discussions. We are grateful to Professor J. R. Chelikowsky and Dr. S. Öğüt for sharing with us their DFT codes and computational advice. This research was supported by the National Science Foundation, the US Army Research Office, and the Office of Basic Energy Sciences.

[1] M. F. Jarrold, J. Phys. Chem. **99**, 11 (1995).
[2] G. von Helden, M. T. Hsu, P. R. Kemper, and M. T. Bowers, J. Chem. Phys. **95**, 3835 (1991).
[3] G. von Helden, M. T. Hsu, N. G. Gotts, and M. T. Bowers, J. Phys. Chem. **97**, 8182 (1993).
[4] K. B. Shelimov, J. M. Hunter, and M. F. Jarrold, Int. J. Mass Spectrom. Ion Processes **138**, 17 (1994).
[5] J. M. Hunter, J. L. Fye, and M. F. Jarrold, Science **260**, 784 (1993).
[6] J. M. Hunter, J. L. Fye, and M. F. Jarrold, J. Chem. Phys. **99**, 1785 (1993).
[7] J. M. Hunter, J. L. Fye, E. J. Roskamp, and M. F. Jarrold, J. Phys. Chem. **98**, 1810 (1994).
[8] S. Lee, N. G. Gotts, G. von Helden, and M. T. Bowers, J. Phys. Chem. A **101**, 2096 (1997).
[9] G. von Helden, E. Porter, N. G. Gotts, and M. T. Bowers, J. Phys. Chem. **99**, 7707 (1995).
[10] J. L. Fye and M. F. Jarrold, J. Phys. Chem. A **101**, 1836 (1997).
[11] S. Lee, N. G. Gotts, G. von Helden, and M. T. Bowers, Science **267**, 999 (1995).
[12] K. B. Shelimov and M. F. Jarrold, J. Phys. Chem. **99**, 17677 (1995); J. Am. Chem. Soc. **118**, 1139 (1996).
[13] K. B. Shelimov, D. E. Clemmer, and M. F. Jarrold, J. Chem. Soc. Dalton Trans. **5**, 567 (1996).
[14] J. L. Fye and M. F. Jarrold, Int. J. Mass Spectrom. **187**, 507 (1999).
[15] M. F. Jarrold and J. E. Bower, J. Chem. Phys. **98**, 2399 (1993).
[16] M. F. Jarrold and J. E. Bower, J. Phys. Chem. **97**, 1746 (1993).
[17] M. F. Jarrold and V. A. Constant, Phys. Rev. Lett. **67**, 2994 (1991).
[18] M. F. Jarrold and J. E. Bower, J. Chem. Phys. **96**, 9180 (1992).
[19] K. M. Ho, A. A. Shvartsburg, B. C. Pan, Z. Y. Lu, C. Z. Wang, J. G. Wacker, J. L. Fye, and M. F. Jarrold, Nature (London) **392**, 582 (1998).
[20] B. Liu, Z. Y. Lu, B. Pan, C. Z. Wang, K. M. Ho, A. A. Shvartsburg, and M. F. Jarrold, J. Chem. Phys. **109**, 9401 (1998).
[21] J. M. Hunter, J. L. Fye, M. F. Jarrold, and J. E. Bower, Phys. Rev. Lett. **73**, 2063 (1994).
[22] A. A. Shvartsburg, B. Liu, Z. Y. Lu, C. Z. Wang, M. F. Jarrold, and K. M. Ho, Phys. Rev. Lett. **83**, 2167 (1999).
[23] A. A. Shvartsburg and M. F. Jarrold, Phys. Rev. A **60**, 1235 (1999).
[24] S. Lee, T. Wyttenbach, G. von Helden, and M. T. Bowers, J. Am. Chem. Soc. **117**, 10159 (1995).
[25] R. R. Hudgins, Y. Mao, M. A. Ratner, and M. F. Jarrold, Biophys. J. **76**, 1591 (1999).
[26] R. R. Hudgins, M. A. Ratner, and M. F. Jarrold, J. Am. Chem. Soc. **120**, 12974 (1998).
[27] K. B. Shelimov and M. F. Jarrold, J. Am. Chem. Soc. **118**, 10313 (1996); *ibid.* **119**, 2987 (1997).
[28] M. F. Jarrold, Acc. Chem. Res. **32**, 360 (1999).
[29] S. J. Valentine, J. G. Anderson, A. D. Ellington, and D. E. Clemmer, J. Phys. Chem. B **101**, 3891 (1997).
[30] E. Mack, Jr., J. Am. Chem. Soc. **47**, 2468 (1925).
[31] A. A. Shvartsburg and M. F. Jarrold, Chem. Phys. Lett. **261**, 86 (1996).
[32] M. F. Mesleh, J. M. Hunter, A. A. Shvartsburg, G. C. Schatz, and M. F. Jarrold, J. Phys. Chem. **100**, 16082 (1996).
[33] A. A. Shvartsburg, G. C. Schatz, and M. F. Jarrold, J. Chem. Phys. **108**, 2416 (1998).
[34] A. A. Shvartsburg, R. R. Hudgins, Ph. Dugourd, and M. F. Jarrold, J. Phys. Chem. A **101**, 1684 (1997).
[35] A. A. Shvartsburg, R. R. Hudgins, R. Gutierrez, G. Jungnickel, T. Frauenheim, K. A. Jackson, and M. F. Jarrold, J. Phys. Chem. A **103**, 5275 (1999).
[36] A. A. Shvartsburg, L. A. Pederson, R. R. Hudgins, G. C. Schatz, and M. F. Jarrold, J. Phys. Chem. A **102**, 7919 (1998).
[37] A. A. Shvartsburg, R. R. Hudgins, Ph. Dugourd, R. Gutierrez, T. Frauenheim, and M. F. Jarrold, Phys. Rev. Lett. (in press).
[38] Ph. Dugourd, R. R. Hudgins, and M. F. Jarrold, Chem. Phys. Lett. **267**, 186 (1997).
[39] R. R. Hudgins, Ph. Dugourd, J. M. Tenenbaum, and M. F. Jarrold, Phys. Rev. Lett. **78**, 4213 (1997).
[40] J. P. K. Doye and D. J. Wales, Phys. Rev. B **59**, 2292 (1999).
[41] N. G. Gotts, G. von Helden, and M. T. Bowers, Int. J. Mass Spectrom. Ion Processes **149/150**, 217 (1995).
[42] Ph. Dugourd, R. R. Hudgins, J. M. Tenenbaum, and M. F. Jarrold, Phys. Rev. Lett. **80**, 4197 (1998).
[43] W. Ekardt, Phys. Rev. B **29**, 1558 (1984).
[44] J. Lerme, Ph. Dugourd, R. R. Hudgins, and M. F. Jarrold, Chem. Phys. Lett. **304**, 19 (1999).
[45] S. M. Reimann, S. Frauendorf, and M. Brack, Z. Phys. D: At., Mol. Clusters **34**, 125 (1995).
[46] M. Koskinen, P. O. Lipas, and M. Manninen, Z. Phys. D: At., Mol. Clusters **35**, 285 (1995).
[47] R. R. Hudgins, M. Imai, M. F. Jarrold, and Ph. Dugourd, J. Chem. Phys. **111**, 7865 (1999).
[48] A. A. Shvartsburg, M. F. Jarrold, B. Liu, Z. Y. Lu, C. Z. Wang, and K. M. Ho, Phys. Rev. Lett. **81**, 4616 (1998).
[49] C. Z. Wang, B. C. Pan, and K. M. Ho, J. Phys.: Condens. Matter **11**, 2043 (1999).
[50] R. Car and M. Parrinello, Phys. Rev. Lett. **55**, 2471 (1985).
[51] DMOL package, 96.0/4.0.0 (MSI, San Diego, 1996).
[52] R. Kishi, Y. Negishi, H. Kawamata, S. Iwata, A. Nakajima, and K. Kaya, J. Chem. Phys. **108**, 8039 (1998).
[53] M. Woeller, M. Mühlhäuser, S. D. Peyerimhoff, and F. Grein, Chem. Phys. Lett. **288**, 603 (1998).
[54] B. Liu (unpublished).
[55] K. Jackson, M. Pederson, C. Z. Wang, and K. M. Ho, Phys. Rev. A **59**, 3685 (1999).
[56] N. Binggeli and J. R. Chelikowsky, Phys. Rev. Lett. **75**, 493 (1995).
[57] J. R. Chelikowsky and N. Binggeli, Mater. Sci. Forum **232**, 87 (1996).
[58] S. Öğüt and J. R. Chelikowsky, Phys. Rev. B **55**, R4914 (1997).
[59] K. Raghavachari and C. M. Rohlfing, J. Chem. Phys. **94**, 3670 (1991).
[60] C. M. Rohlfing and K. Raghavachari, J. Chem. Phys. **96**, 2114 (1992).
[61] L. A. Curtiss, P. W. Deutsch, and K. Raghavachari, J. Chem. Phys. **96**, 6868 (1992).
[62] R. Kishi, H. Kawamata, Y. Negishi, S. Iwata, A. Nakajima, and K. Kaya, J. Chem. Phys. **107**, 10029 (1997).
[63] R. Kishi, S. Iwata, A. Nakajima, and K. Kaya, J. Chem. Phys. **107**, 3056 (1997).
[64] O. Chesnovsky, S. H. Yang, C. L. Pettiette, M. J. Craycraft, Y. Liu, and R. E. Smalley, Chem. Phys. Lett. **138**, 119 (1987).
[65] T. N. Kitsopoulos, C. J. Chick, A. Weaver, and D. M. Neumark, J. Chem. Phys. **93**, 6108 (1990).

[66] C. C. Arnold and D. M. Neumark, J. Chem. Phys. **99**, 3353 (1993); *ibid.* **100**, 1797 (1994).
[67] G. Schulze Icking-Konert, H. Handschuh, P. S. Bechtold, G. Ganteför, B. Kessler, and W. Eberhardt, Surf. Rev. Lett. **3**, 483 (1996).
[68] C. Xu, T. R. Taylor, G. R. Burton, and D. M. Neumark, J. Chem. Phys. **108**, 1395 (1998).
[69] I. Vasiliev, S. Öğüt, and J. R. Chelikowsky, Phys. Rev. Lett. **78**, 4805 (1997).
[70] A. Sieck, D. Porezag, T. Frauenheim, M. R. Pederson, and K. Jackson, Phys. Rev. A **56**, 4890 (1997).
[71] C. M. Rohlfing and K. Raghavachari, Chem. Phys. Lett. **167**, 559 (1990).
[72] All mobilities calculated in this paper are for the PWB-optimized geometries. This marginally differs from Ref. 20, where we had used the average between PWB and BLYP structures. This change has been made because PWB produces by far the best agreement with the measured dissociation energies and fragmentation pathways (Ref. 48).
[73] In fact, the slight discrepancies between the mobilities for some Si_n^+ calculated here and in Ref. 20 are mostly due not to a different method of mobility calculations, but to a marginally different method of geometry optimization (Ref. 72).
[74] This does not imply that the trajectory calculations are of little extra value in the analysis of mobility measurements for ions with large interatomic distances. It is always better to make the structural assignments of features resolved in these measurements on the basis of a set of mobilities at different temperatures, rather than a single value. Modeling the dependence of mobility on temperature requires the trajectory calculations. They are also needed to account for the spatial distribution of ionic charge, which has proved to be important for the mobilities at low temperatures (Ref. 20).
[75] A. A. Shvartsburg and M. F. Jarrold (unpublished).
[76] The values of $E_{cut}=3\times10^{-3}$ for Si_n^+ and $E_{cut}=2.6\times10^{-3}$ for Si_n^- [in units of elementary charge/(atomic unit)^3] have been set by fitting, using PWB, the mobilities for, respectively, Si_7^+ and Si_7^- measured (Ref. 47) at 295 K.
[77] V. Queneau, E. Todorov, and S. C. Sevov, J. Am. Chem. Soc. **120**, 3263 (1998).
[78] K. Raghavachari and C. M. Rohlfing, J. Chem. Phys. **89**, 2219 (1988).
[79] K. Raghavachari, Z. Phys. **12**, 61 (1989).
[80] K. Raghavachari and C. M. Rohlfing, Chem. Phys. Lett. **198**, 521 (1992).
[81] K. Raghavachari, Phase Transit. **24–26**, 61 (1990).
[82] J. R. Chelikowsky and J. C. Phillips, Phys. Rev. Lett. **63**, 1653 (1989).
[83] J. R. Chelikowsky and J. C. Phillips, Phys. Rev. B **41**, 5735 (1990).
[84] J. C. Phillips, Phys. Rev. B **47**, 14132 (1993).
[85] T. Lange and T. P. Martin, Angew. Chem. Int. Ed. Engl. **31**, 172 (1992).
[86] E. Kaxiras and K. A. Jackson, Phys. Rev. Lett. **71**, 727 (1993).
[87] E. Kaxiras and K. A. Jackson, Z. Phys. D: At., Mol. Clusters **26**, 346 (1993).
[88] M. R. Pederson, K. Jackson, D. V. Porezag, Z. Hajnal, and T. Frauenheim, Phys. Rev. B **54**, 2863 (1996).
[89] J. C. Grossman and L. Mitas, Phys. Rev. Lett. **74**, 1323 (1995).
[90] J. C. Grossman and L. Mitas, Phys. Rev. B **52**, 16735 (1995).
[91] C. H. Patterson and R. P. Messmer, Phys. Rev. B **42**, 7530 (1990).